Electronic Supplementary Material (ESI) for Journal of Materials Chemistry A.

Supporting Information

Network-like Mesoporous $NiCo_2O_4$ Grown on Carbon Cloth for High-Performance Pseudocapacitors

Suning Gao, Fan Liao*, Shuzhen Ma, Lili Zhu, Mingwang Shao*

Jiangsu Key Laboratory for Carbon-Based Functional Materials & Devices, Institute of Functional Nano & Soft Materials (FUNSOM), Soochow University, Suzhou 215123, P. R. China.

1. Materials Characterization.

The phase and crystallography of samples were characterized by XRD (Philips X'pert PRO MPD diffractometer) equipped with Cu Kα radiation (λ = 0.15406 nm). The morphology of samples was examined by scanning electron microscopy (SEM, FEI-quanta 200 scanning electron microscope) equipped with EDAX and a Zeiss Supra 55 field scanning electron microscopy. Transmission electron microscope (TEM) image and high resolution TEM (HRTEM) image were recorded using a FEI Tecnai F20 transmission electron microscope with accelerating voltage of 200 kV. The chemical states of the products were studied using the X-ray photoelectron spectroscopy (XPS) measurement performed on Kratos AXIS UltraDLD ultrahigh vacuum surface analysis system) with Al Kα radiation (1486 eV) as probe and an indium plate as the supporter of the powder samples. The Brunauere-Emmette-Teller (BET) specific surface area and the pore size distribution of these samples were investigated by the ASAP 2020 instrument at 77 K. The mass of electrode materials was weighed on a XS analytical balance (Mettler Toledo; δ = 0.01 mg).

2. Electrochemical Measurements.

An electrolyte of 3 M KOH aqueous solution was used at room temperature. The CC supported electroactive material serves directly as the working electrode. Pt wire and a saturated calomel electrode (SCE) were used as the counter electrode and the reference electrode, respectively. EIS tests were made with a superimposed 5 mV sinusoidal voltage in the frequency range from 100 kHz-0.01 Hz.

3. XRD pattern of bare CC substrate and EDS spectrum of the NWM $NiCo_2O_4$.

Fig. S1a shows XRD pattern of the bare substrate CC, all peaks can be indexed tographite (JCPDS data No. 08-0415). EDS spectrum indicates that the atomic ratio of Co: Ni is 1.9 : 1, further confirming the results concluded from XRD and XPS.

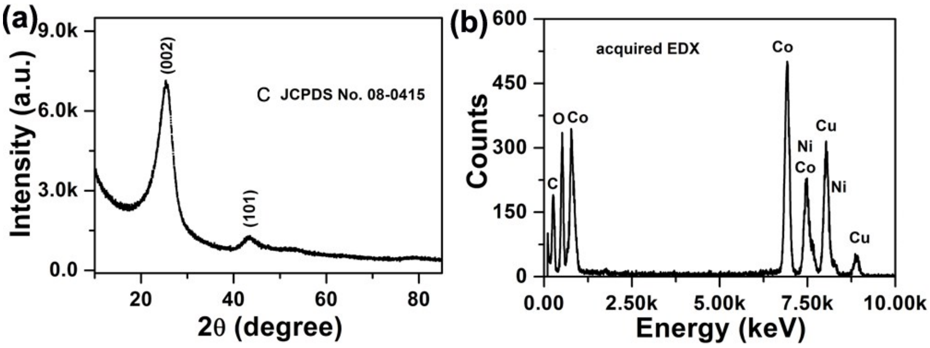

Fig. S1. (a) XRD pattern of the bare substrate CC; and (b) EDS spectrum of the NWM $NiCo_2O_4$.

4. SEM images of $NiCo_2O_4$ with and without the capping agents.

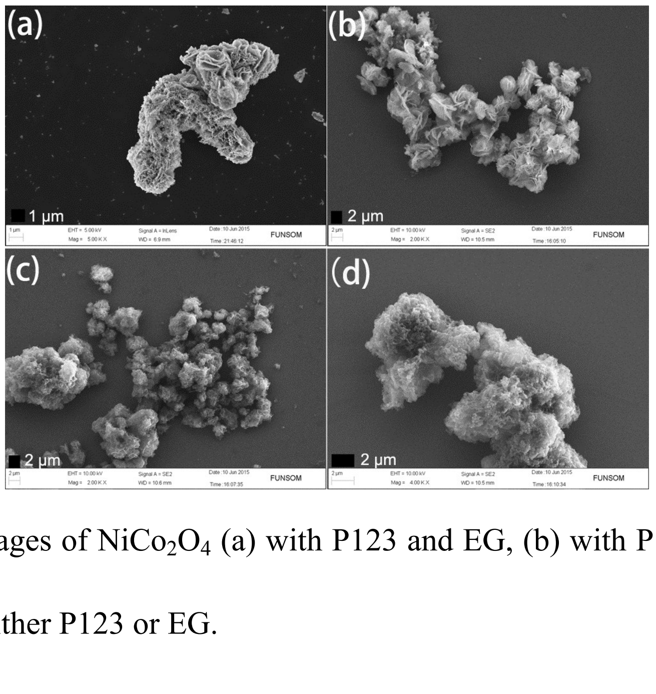

Fig. S2. SEM images of $NiCo_2O_4$ (a) with P123 and EG, (b) with P123, (c) with EG, and (d) without either P123 or EG.

5. SEM images of NWM $NiCo_2O_4$ on CC with different reaction times.

Fig. S3a shows some separate and small nanoflakes were formed at the beginning of the hydrothermal reaction. With the prolonged time, more nanoflakes coupled with bigger size were noticed. Three dimensional net-works like structures composed of highly uniform nanoflakes were formed as shown in Fig. S3c. When the reactive time reached to 4h, the formed structures also can be observed without obvious change.

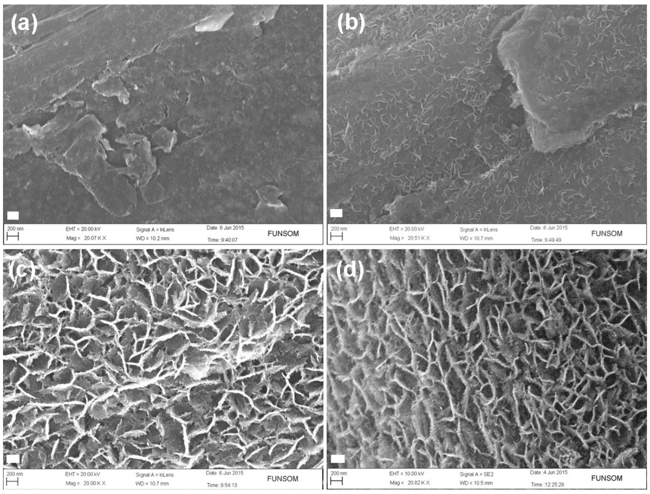

Fig. S3. SEM images of NWM $NiCo_2O_4$ on CC with different reaction times: (a) 0.5 h, (b) 1 h, (c) 2 h, and (d) 4 h, respectively. The scale bar is 200 nm.

6. BET and BJH of NiO NSs

Fig. S4 exhibits BET and BJH patterns with surface area of 108.6 m^2/g and a major pore size distribution ranging from 2 to 5 nm.

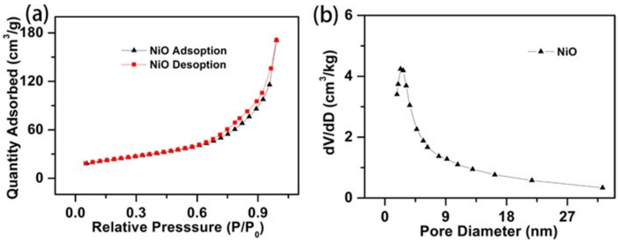

Fig. S4. (a) BET and (b) BJH of NiO NSs.

7. CV and GCD curves of NiO NSs

Fig. S5a displays the CV curves at different scaning rates of NiO NSs array electrode, revealing the pseudocapacitive nature of the as-prepared sample. The potential of the redox peaks is not the same as that of $NiCo_2O_4$ due to the occurring of different faradaic pseudocapacitance reation $NiO + OH^- \leftrightarrow NiOOH + e^-$.[S1] Fig. S5b studies the GCD curves of NiO NSs at various current densities with asymmetric profile may attributed to polarization of the electrode.

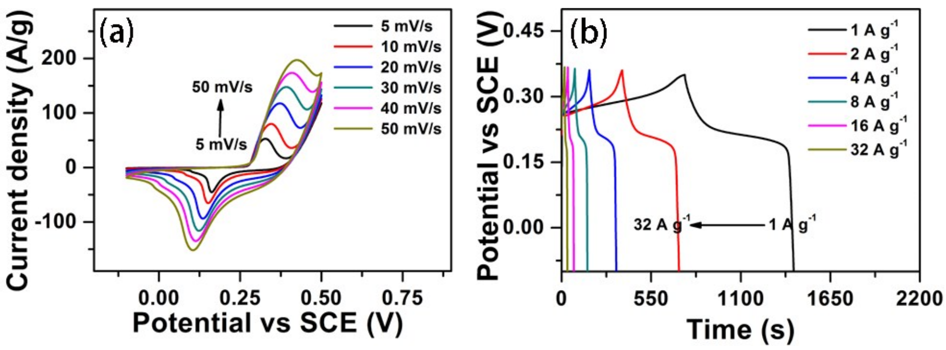

Fig. S5. (a) CV and (b) GCD curves of NiO NSs at different scaning rates and various current densities.

8. Specific capacitances as a function of scan rates of CV

The SCs decrease with increasing scan rates (Fig. S6) due to the existing of some inaccessible active surface areas for charge storage at a high scan rate.

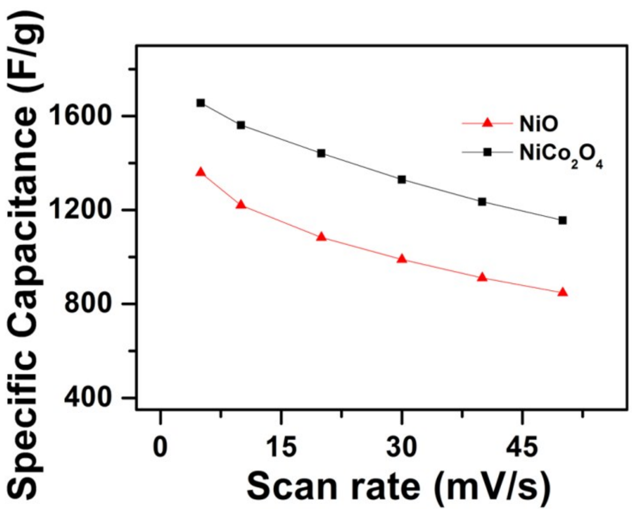

Fig. S6. Specific capacitances as a function of scan rates of CV.

9. CV of bare CC substrate and the curve controlled by diffusion in electrode reaction of $NiCo_2O_4$.

Fig. S7a shows CV of bare CC substrate at a scan rate of 10 mV/s with a capacitance calculated from formula (1) is nearly 1.8 F, while the capacitance of the $NiCo_2O_4$/CC electrode is 608.2 F with a 0.33 mg loading. Fig. S7b reveals a linear behavior of peak current density and the square root of the scan rate of $NiCo_2O_4$.

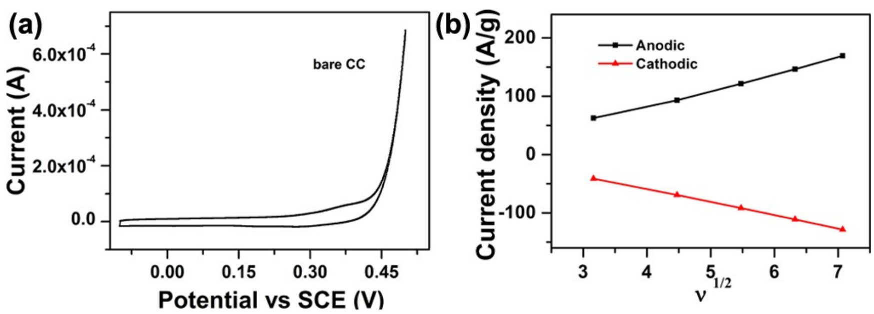

Fig. S7. (a) CV of bare CC substrate; and (b) the curve controlled by diffusion in electrode reaction of $NiCo_2O_4$.

10. First 10 cycles of GCD curves of NWM $NiCo_2O_4$.

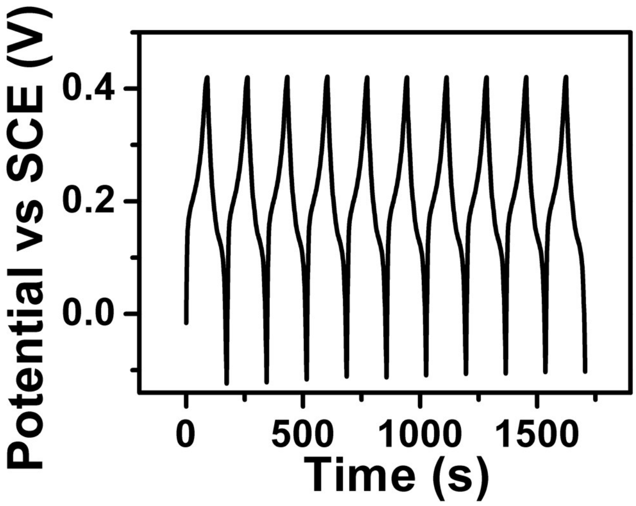

Fig. S8. First 10 cycles of GCD curves of NWM $NiCo_2O_4$.

11. Cycling performance of NiO electrode

The total capacitance loss of NiO electrodeafter 4000 cycles is around 20%, much worse than that of NWM $NiCo_2O_4$, is exhibited in Fig. S9.

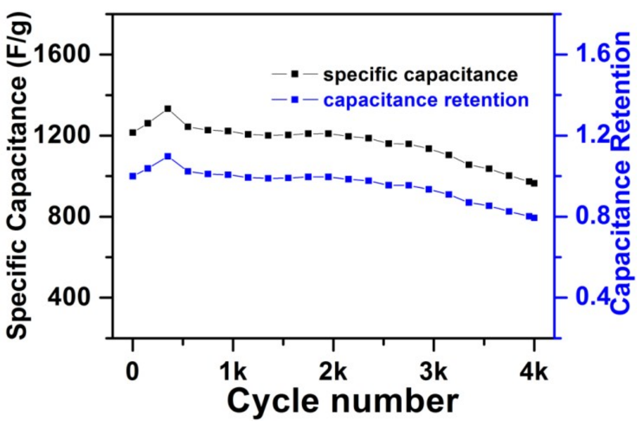

Fig. S9. Cycling performance of NiO NSs electrode.

12. Cycling performance of NWM $NiCo_2O_4$ symmetric device.

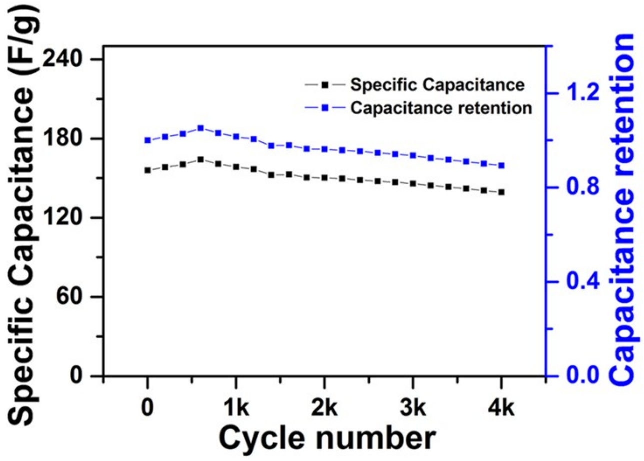

Fig. S10. Cycling performance of NWM $NiCo_2O_4$ symmetric device calculated by repeated CD curves at a current density of 10 A/g.

13. The comparison of specific capacitance, capacitance retention and rate capability of the various $NiCo_2O_4$ samples.

Table S1. The comparison of specific capacitance, capacitance retention and rate capability of the network $NiCo_2O_4$ in this work and those of other nanostructured spinel electrode materials reported in the previous works.

Morphology	Capacitane	Rate capability	Cycling stability	Mass loading mg/cm^2	Ref.
nanowall-network $NiCo_2O_4$	1225 F/ g (5 A/g)	81.3 % (5 A/g to 40 A/g)	79% (2000 cycles)	0.0625	S2
Urchin-like $NiCo_2O_4$	1650 F/g (1 A/g)	81 % (1 A/g to 15 A/g)	90 % (2000 cycles)	-	S3
Flower-Shaped $NiCo_2O_4$ Microsphere	1006 F/g (1 A/g)	72.2% (1 A/g to 20 A/g)	93.2 % (1000 cycles)	3.0	S4

Hierarchical porous network-like $NiCo_2O_4$	587 F/g (1 A/g)	-	94 % (3500 cycles)	5	S5
$NiCo_2O_4$ nanosheets	796 F/g (1 A/g)	-	87.1 % (2400 cycles)	0.8	S6
Hierarchical mesoporous $NiCo_2O_4$	1619.1 F/g (2 A/g)	35.3 % (2 A/g to 10 A/g)	-	-	S7
Chain-like $NiCo_2O_4$ nanowires	1284 F/g (2 A/g)	76.8 % (2 A/g to 20 A/g)	97.5% (3000 cycles)	-	S8
Hierarchical $NiCo_2O_4$@$NiCo_2O_4$	895 F/g	76.5 % (1 A/g to 20 A/g)	73.2% (2000 cycles)	1.97	S9
NWM $NiCo_2O_4$	1843 F/g (1 A/g)	80% (1 A/g to 32 A/g)	90% (4000 cycles)	0.33	This work

14. The values of R_e, R_{ct}, C_{dl}, W and C_{ps} of NWM $NiCo_2O_4$ and NiO NS.

Table S2. The values of equivalent series resistance R_e, charge-transfer resistance R_{ct}, double-layer capacitance C_{dl}, Warburg resistance W and pseudocapacitive element C_{ps} simulated by ZsimpWin software of NWM $NiCo_2O_4$ and NiO NS.

	R_e [ohm·cm^2]	R_{ct} [ohm·cm^2]	C_{dl} [F/cm^2]	W [S·sec^5/cm^2]	C_{ps} [F/cm^2]
NWM $NiCo_2O_4$	1.041	0.5059	1.041E-5	0.2664	0.3476
NiO NS	0.8505	2.41	0.001198	0.1205	0.2576

REFERENCES

S1 D. T. Dam, X. Wang and J. M. Lee, *Nano Energy.*, 2013, **2**, 1303-1313.

S2 N. Padmanathan and S. Selladurai, *RSC Adv.*, 2014, **4**, 8341-8349.

S3 Q. F. Wang, B. Liu, X. F. Wang, S. H. Ran, L. M. Wang, D. Chen and G. Z. Shen, *J. Mater. Chem.*, 2012, **22**, 21647-21653.

S4 Y. Lei, J. Li, Y. Y. Wang, L. Gu, Y. F. Chang, H. Y. Yuan and X. Dan, *ACS Appl. Mater. Interfaces*, 2014, **6**, 1773-1780.

S5 C. Yuan, J. Li, L. Hou, J. Lin, X. Zhang and S. Xiong, *J. Mater. Chem. A*, 2013, **1**, 11145-11151.

S6 F. Z. Deng, L. Yu, M. Sun, T. Lin, G. Cheng, B. Lan and F. Ye, *Electrochim. Acta*, 2014, **133**, 382-390.

S7 Y. F. Zhang, M. Z. Ma, J. Yang, H. Q. Su, W. Huang and X. C. Dong, *Nanoscale*, 2014, **6**, 4303-4308.

S8 R. Zou, K. Xu, T. Wang, G. He, Q. Liu, X. Liu, Z. Zhang and J. Q. Hu, *J. Mater. Chem. A*, 2013, **1**, 8560-8566.

S9 X. Liu, S. Shi, Q. Xiong, L. Li, Y. Zhang, H. Tang, C. Gu, X. Wang and J. Tu, *ACS Appl. Mater. Interfaces*, 2013, **5**, 8790-8795.